PHOTOACOUSTIC SPECTROSCOPY OF BACTERIORHODOPSIN PHOTOCYCLE

MICHEL RENARD, PATRICE THIRION, AND MICHEL DELMELLE
Physique Experimentale, Institut de Physique, Université de Liège, 400 Sart-Tilman, Belgium

ABSTRACT Photoacoustic spectroscopy was applied to study the energetics and the kinetics of the slow intermediates of the bacteriorhodopsin photocycle. An analysis of the modulation frequency dependence of the photoacoustic signal allowed us to estimate the enthalpy changes and the kinetic parameters associated with those intermediates. The effects of pH, salt concentration, and protein aggregation were studied. Three photoacoustic transitions were found. The two low frequency transitions were attributed to O_{660} and M_{412}, respectively. The third transition was interpreted as resulting from a protein conformational change undetected spectrophotometrically. The frequency spectra were simulated between 5 and 180 Hz at pH's 5.1, 7.0, and 8.9 assuming a branching in the bacteriorhodopsin photocycle at the M_{412} level. The enthalpy changes associated with M_{412} and O_{660} were computed and compared with the experimental values.

INTRODUCTION

Bacteriorhodopsin (BR) is the protein-pigment complex found in the purple membrane of *Halobacterium halobium* (for a review, see references 1 and 2). Absorption of a photon by the light-adapted form of bacteriorhodopsin initiates a photocycle during the course of which protons are translocated across the purple membrane. Nagle et al. (3) have shown that the interpretation of the light-induced absorption changes is not unambiguous. Initially, the photocycle was thought to be linear ($BR_{570} \longrightarrow K_{590} \longrightarrow L_{550} \longrightarrow M_{412} \longrightarrow O_{660} \longrightarrow BR_{570}$) (4), but Dencher and Wilms (5) and more recently Lozier et al. (6), Sherman et al. (7), and Renard and Delmelle (8) provided some experimental evidence supporting a branched model. Although many kinetic models have been proposed (3), some interconnections between the intermediates are still equivocal.

The energy variations associated with the intermediate formation have been barely investigated. Very little is known about the thermodynamics of the conversion of visible light into chemical energy. Two experimental techniques were used to approach the problem. Ort and Parson (9) used a capacitor microphone calorimeter and measured rapid enthalpy changes occurring during the bacteriorhodopsin photocycle. Garty et al. (10, 11), on the other hand, applied photoacoustic (PA) spectroscopy to follow the kinetics of heat production during the photochemical reactions occurring on a millisecond timescale. Identification of spectral regions with varying photoactivities allowed the authors to estimate the energy stored in the intermediates. The modulation frequency dependence yielded information about the chronology and the extent of the enthalpy changes. Although Garty et al. (10) considered the possibility of a branching, they discussed their results in terms of a linear model.

In the present study, the PA frequency spectra of purple membrane suspensions are described with special emphasis on the effects of pH, salt concentration, and protein aggregation. The data are analyzed quantitatively by applying the theoretical background established by Malkin and Cahen (12) to a branched photocycle. The enthalpy changes associated with the slow intermediates are evaluated on that basis.

MATERIALS AND METHODS

PA Measurements

Purple membrane suspensions were introduced into a closed aluminium chamber similar to the one described by Ducharme et al. (13). The sample was illuminated with a 300-W xenon lamp (VIX 300 UV; Varian Associates, Inc., Palo Alto, CA). The light beam was modulated by a mechanical chopper (model 192; EG&G Princeton Applied Research, Princeton, NJ) between 5 and 420 Hz. The light was focused through a cylindrical lens on the aperture slit of a monochromator (f/3.5; Farrand Optical Co. Inc., Valhalla, NY) adjusted at 570 ± 10 nm. The light flux on the sample was 110 W/m^2. A pyrodetector was used to monitor the variations of the light intensity.

Heat was generated in the outermost layer of the membrane suspension following the absorption of monochromatic light. The sample layer that contributes to the PA signal is approximately given by $(2\alpha/\omega)^{1/2}$, where α is the thermal diffusivity (14). The pressure modulation within the closed chamber was detected by a microphone (type 4166; Brüel et Kjaer Ltd., Naerum, Denmark) to which was directly connected a preamplifier (type 2619; Brüel et Kjaer Ltd.). The output signal was then fed into a lock-in amplifier (model 5204; EG&G Princeton Applied Research). The reference signal came from the mechanical chopper. Its frequency was precisely measured with a CMC 608 frequency meter (Pacific Industries Inc; Computer Measurements Co; San Fernando, CA). The PA signal was recorded with a 3-s time constant against the chopper frequency.

The determination of the enthalpy changes associated with bacterio-

rhodopsin intermediates required a photoinactive reference sample (10). A bleached purple membrane suspension mixed with black ink was used to match the optical and thermal properties of the photoactive sample. The bleaching was performed in the presence of NH_2OH as previously described (15).

The lock-in amplifier phase was adjusted at each modulation frequency to obtain a maximal in-phase signal with the reference sample. This phase value was adopted for recording the in-phase PA spectra from the photoactive samples. The magnitude signal represents the square root of the sum of the squared in-phase and out-of-phase components. Actually, a signal was detected at the microphone output even when the wavelength of illumination was not absorbed by the sample. This background signal was systematically measured at 700 nm for each frequency of modulation. It was then substracted from the 570-nm signal.

Materials

Purple membrane fragments from *Halobacterium halobium* (strain R_1M_1) were isolated as previously described (16). They were suspended in 66 mM phosphate or Tris-HCl buffer with or without 4 M NaCl. The bacteriorhodopsin concentration was 7.5×10^{-4} M as determined at 570 nm with a spectrophotometer (559; Perkin-Elmer Corp., Coleman Instrument Div., Oak Brook, IL) ($\epsilon = 63{,}000\ M^{-1}cm^{-1}$), using quartz cells with a 0.1-mm light path. 80 μl aliquots were used for each photoacoustic measurement.

The purple membrane solubilization was carried out at room temperature for 48 h, using Triton X-100 as a detergent. The protein-detergent ratio was 1:35 (wt/wt) in 66 mM phosphate buffer, pH 5.1. Solubilization shifted the absorption maximum to 550 nm but no new band appeared at 380 nm, indicating the lack of any chromophore loss (17). During the PA measurements at pH 5.1, a 5% bleaching was systematically observed. This 5% reduction of the signal amplitude was taken into account in the evaluation of the data.

Simulation

The PA frequency spectra were simulated on a TRS-80 microcomputer (model I, Basic Microsoft level II; Radio Shack, Tandy Corp., Fort Worth, TX). The experimental and the theoretical curves were fitted using the least-square method. All the experimental values were taken into account in the fitting procedure.

RESULTS

Experimental Results

Malkin and Cahen (12) have established a relationship between the PA signal intensity (ρ) and the energy variations associated with the formation of the photochemical products.

$$\rho = K(\omega) \cdot I(\omega, \lambda) \cdot (Nh\nu - \Sigma_i \phi_i \Delta E_i) . \qquad (1)$$

$I(\omega, \lambda)$ is the light absorbed by the thermally active layer (see Materials and Methods) at wavelength λ and chopping angular velocity ω; K is a constant that depends upon the instrument and the sample. N, h, and c are the Avogadro's and Planck's constants, and the speed of light, respectively. ϕ_i and ΔE_i are the quantum yield and the internal energy change associated with the formation of intermediate i. The summation is extended over the intermediates that store energy for periods longer than $1/\omega$. The expression $\Sigma_i \phi_i \Delta E_i$ is therefore frequency and wavelength dependent. Its determination implies a precise evaluation of K and of $I(\omega, \lambda)$. The best approach is to use a suitable nonphotoactive reference for which $\phi_i = 0$ (10). In those conditions, the PA signal is $\rho_{ref} = K(\omega) \cdot I(\omega, \lambda) \cdot Nh\nu$, and Eq. 1 can be rewritten

$$\rho/\rho_{ref} = 1 - \frac{\Sigma_i \phi_i \Delta E_i}{Nh\nu} \qquad (2)$$

since $K(\omega) \cdot I(\omega, \lambda)$ is identical for the two samples. ρ/ρ_{ref} represents the ratio of the heat dissipated in the photoactive sample to that dissipated in the photoinactive sample. Neither ϕ_i nor ΔE_i are directly accessible experimentally. The measurement of the ratio, ρ/ρ_{ref}, allows only to evaluate $\Sigma_i \phi_i \Delta E_i$.

Our measurements were performed on purple membrane sheets dispersed in buffer ($c = 7.5 \times 10^{-4}$M). Samples were illuminated at 570 nm since this wavelength corresponds to the maximal absorption of bacteriorhodopsin. The chopping frequency was varied from 5 to 420 Hz. At higher frequencies, the signal-to-noise ratio deteriorated rapidly. The reference sample consisted of a bleached membrane suspension (see Materials and Methods section).

Figs. 1 and 2 show the influence of the chopping frequency on the amount of dissipated heat. The frequency spectra were measured at pH 5.1, 7.0, and 8.9. Fig. 1 concerns the in-phase signals, the phase being defined with respect to the inactive sample (see Materials and Methods section). Fig. 2 shows the variations of the magnitude signal. In both figures, at 5 Hz, $\rho = \rho_{ref}$ as expected since at low frequencies all energy is eventually recovered as heat, $1/\omega$ being longer than the photocycle itself. Increasing the chopping frequency reduces the amount of heat dissipated and at 420 Hz, $\rho_{in} = 0.8 \times \rho_{in}^{ref}$ (in-phase) and $\rho_M = 0.88 \times \rho_M^{ref}$ (magnitude). The complex patterns observed between 5 and 420 Hz are associated with the formation of the intermediates (12). Each experimental value is subjected to large errors owing to the low sensitivity of the technique and to the corrections that have to be made. Therefore, it was necessary to adopt a quantitative test for the definition of a transition in a given pattern; a variation larger than the SEM was considered as a transition. Each value in Figs. 1 and 2 represents the mean over at least five different experiments. Three transitions are detected. Their frequencies are given in Table I for the in-phase and the magnitude signals at pH's 5.1, 7.0, and 8.9 respectively. A pH increase reduces the extent of the low frequency transition, since the amount of heat dissipated in the in-phase signal is 87% at pH 5.1 and 94.5% at pH 8.9. At pH 8.9, the low frequency transition is almost unobservable. A similar effect is observed with the magnitude signal.

The second transition is characterized by a lifetime of 2.1 ± 0.1 ms (in-phase). The plateau associated with the end of the transition represents 85.5 ± 1.5% of the dissipated heat. These two values are almost unperturbed

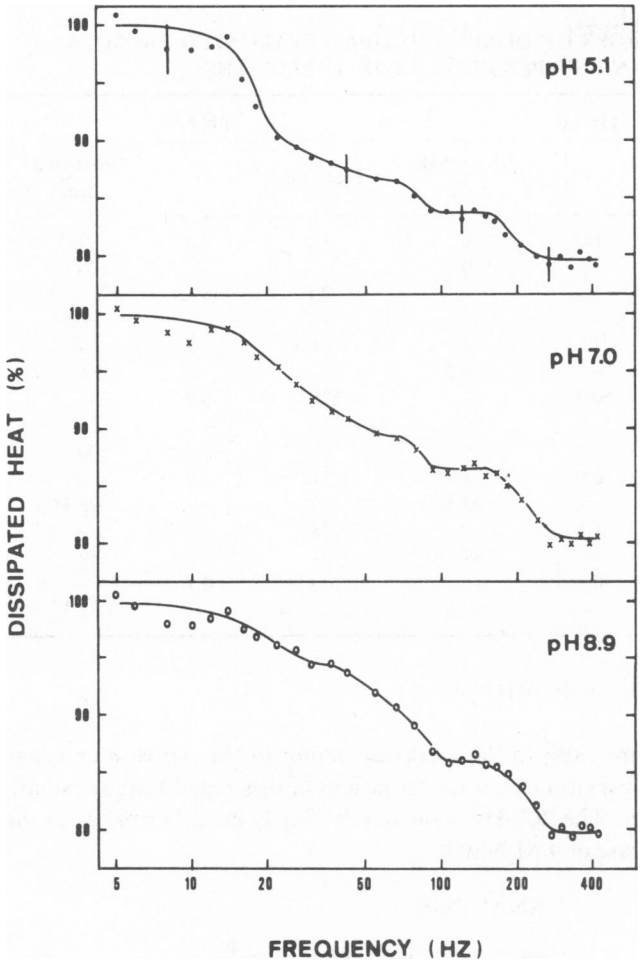

FIGURE 1 Photoacoustic in-phase frequency spectra (5–420 Hz) of purple membrane suspensions (7.5×10^{-4}M) at pH's 5.1, 7.0 (66 mM phosphate buffer), and 8.9 (66 mM Tris-HCl buffer). The in-phase PA signals were measured at 570 nm. The dissipated heat represents the ratio of total heat dissipated in the photoactive sample to that dissipated in the reference sample.

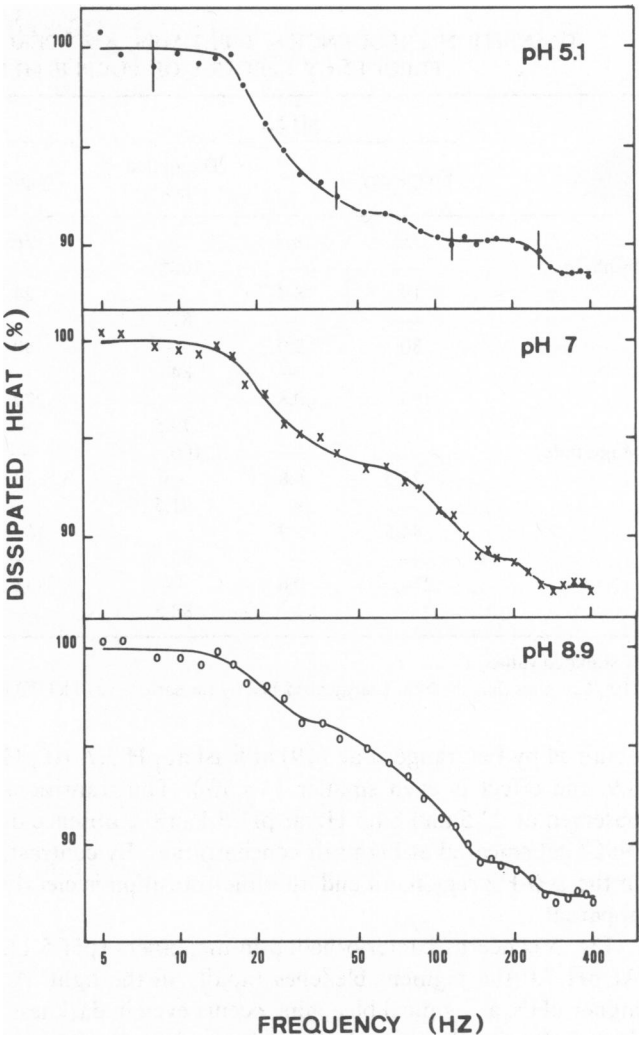

FIGURE 2 Photoacoustic magnitude frequency spectra of purple membrane suspensions (7.5×10^{-4}M) at pH's 5.1, 7.0 (66 mM phosphate buffer), and 8.9 (66 mM Tris-HCl buffer). The magnitude PA signals were measured at 570 nm.

by pH variations. The lifetime associated with the third transition is also pH independent (Table I). Moreover, the plateau that occurs at 80% of dissipated heat remains constant at the three pHs. This indicates that the corresponding $\phi \cdot \Delta E$ is also pH independent.

Malkin and Cahen (12) have previously shown that the appearance of a transition in the frequency spectra can be associated with the formation of an intermediate. The low and middle frequency transitions correspond to lifetimes in the range of 7.6 ± 1.0 and 2.1 ± 0.1 ms, respectively. These values are in agreement with the decay rates of O_{660} (8) and M_{412} (7) as measured by flash photolysis. The 215 ± 20 Hz transition does not correspond to the lifetime of any known intermediate. It could represent a protein conformational change undetected spectrophotometrically (18).

Fig. 3 shows the frequency dependence of the quadrature signal. The reported values were not directly measured, but were computed from the data of Figs. 1 and 2, using the relationship

$$\left(\frac{\rho}{\rho_{ref}}\right)_{quad} = \left[\left(\frac{\rho}{\rho_{ref}}\right)^2_{mag} - \left(\frac{\rho}{\rho_{ref}}\right)^2_{in}\right]^{1/2}. \quad (3)$$

As expected on basis of the analysis carried out by Malkin and Cahen (12), a bell-shaped curve is observed with the quadrature signal when a transition is detected in the in-phase signal. At pH 5.1 (dark dots), maxima are observed at 20, 90, and 300 Hz. An important maximum corresponds to a large transition in the in-phase frequency spectrum. On the contrary, when the in-phase transition is weak (20 Hz, pH 8.9), no maximum is observable in the quadrature signal (clear dots, 20 Hz, Fig. 3).

The effect produced by 4 M NaCl is shown in Fig. 4 in the case of the magnitude signal. The total variation of dissipated heat is inferior to 5% over the whole frequency range. A similar trend seems to occur in the results

TABLE I

TRANSITION FREQUENCIES, LIFETIMES, AND PERCENTAGES OF DISSIPATED HEAT EVALUATED FROM PA FREQUENCY SPECTRA OF PURPLE MEMBRANE SUSPENSIONS AT DIFFERENT pHS

	pH 5.1			pH 7.0			pH 8.9		
	Frequency	τ	Dissipated heat	Frequency	τ	Dissipated heat	Frequency	τ	Dissipated heat
	Hz	*ms*	%	*Hz*	*ms*	%	*Hz*	*ms*	%
In-phase	—	—	100‡	—	—	100	—	—	100
	19	8.4	—	24.5	6.5	—	20	8	—
	—	—	87	—	—	89	—	—	94.5*
	80	2.0	—	80.5	2.0	—	71.5	2.2	—
	—	—	84	—	—	86.5	—	—	86
	195	0.8	—	220	0.7	—	225	0.7	—
	—	—	79.5	—	—	80	—	—	80
Magnitude	—	—	100	—	—	100	—	—	100
	23.5	6.8	—	23	6.9	—	21	7.6	—
	—	—	91.5	—	—	93.5	—	—	96.5*
	84.5	1.9	—	109	1.5	—	88	1.8	—
	—	—	90	—	—	89	—	—	89
	270	0.6	—	233	0.7	—	240	0.7	—
	—	—	88.5	—	—	87.5	—	—	87.5

*Estimated values.

‡100% implies that the light energy absorbed by the sample (210 kJ/E) is entirely dissipated as heat.

obtained by LeGrange et al. (19) at least at pH 7.7. At pH 8.9, the effect is even smaller (≃3.5%). The transitions observed at 23.5 and 84.5 Hz at pH 5.1 in the absence of NaCl get smeared at high salt concentration. By contrast, in the 200-Hz region, an endothermic transition is clearly apparent.

Fig. 5 concerns bacteriorhodopsin monomers (pH 5.1). At pH 7.0 the pigment bleaches rapidly in the light. At higher pH's, a chemical bleaching occurs even in darkness. The slight absorbance reduction observed at pH 5.1 was taken into account in the evaluation of the data. Two transitions are detected at 25 and 81 Hz. These frequencies are close to those corresponding to the native membrane suspensions but the variations of dissipated heat are smaller. The 260-Hz transition is clearly endothermic as in the case of 4 M NaCl.

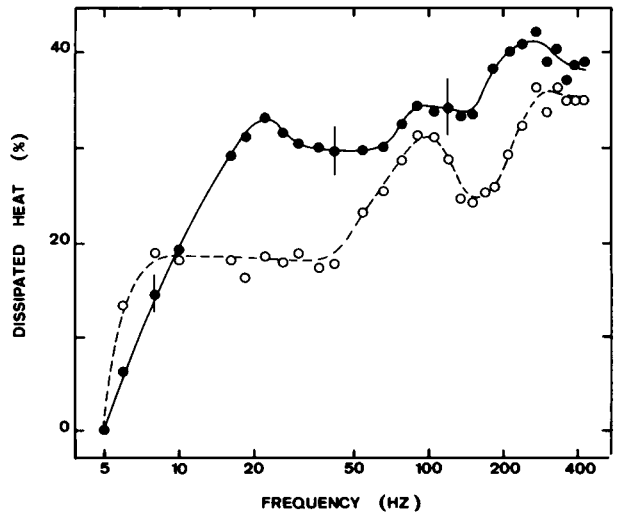

FIGURE 3 Photoacoustic quadrature frequency spectra of purple membrane suspensions at pH's 5.1 (●) and 8.9 (○) in 66 mM buffer. The quadrature PA signals were computed from Figs. 1 and 2.

ANALYSIS

Theoretical Background

A recent analysis of the bacteriorhodopsin photochemistry has outlined the complexity of the photocycle (3). Neither a unidirectional unbranched model nor a unidirectional model with simple branching straight back to BR_{570} from any intermediate is satisfactory for interpreting all experimental data presently available. Lozier et al. (6) have stressed the point that two M-like states seem to be required. Korenstein et al. (20) have even proposed a model involving two L and two M states. At present, any

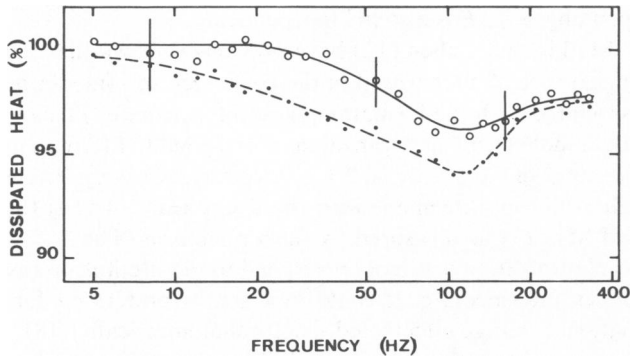

FIGURE 4 Effect of 4 M NaCl on the PA magnitude frequency spectra of purple membrane suspensions at pH's 5.1 (●) and 8.9 (○) in 66 mM buffer. The magnitude PA signals were measured at 570 nm.

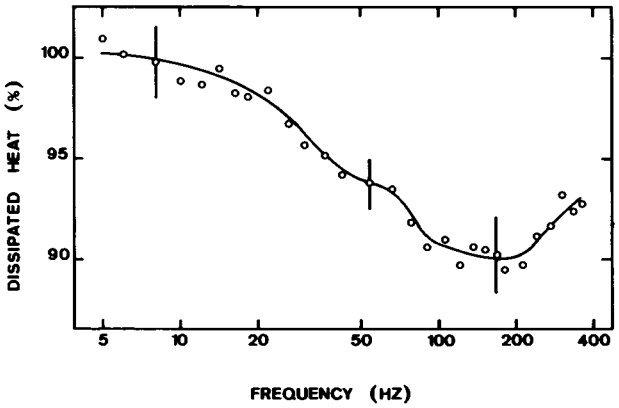

FIGURE 5 Photoacoustic magnitude frequency spectra of bacteriorhodopsin monomers. The purple membrane suspension was solubilized with Triton X-100 in 66 mM buffer at pH 5.1. The magnitude PA signals were measured at 550 nm.

model is open to criticism. The justification of a branched model relies on the observation of the pH effect on the O_{660} formation (7, 8).

The chopping frequency was limited to 420 Hz due to noise problems in the detection system. Hence, intermediates K_{590} and L_{550} were not detectable since their lifetimes fall in the microsecond range. Only the reactions enclosed in the dashed box of Fig. 6 were considered. They

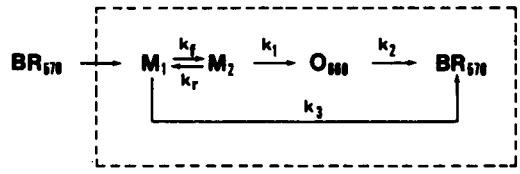

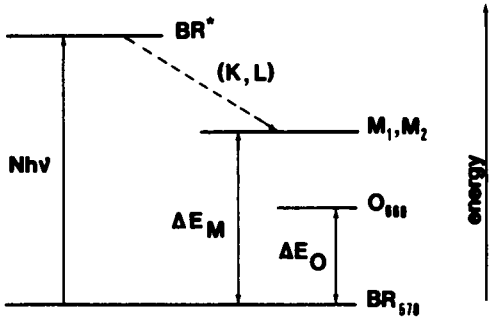

FIGURE 6 *Upper*, branched pathway model of the slow part of the photocycle of bacteriorhodopsin. k_f and k_r describe the forward and reverse transformation between M_1 and M_2. Intermediates K_{590} and L_{550} were not considered in the model. *Lower*, energy diagram of the bacteriorhodopsin photocycle. The photon absorption by BR_{570} leads to the formation of intermediates, M_1 and M_2, with a photochemical quantum yield, ϕ, via intermediates K_{590} and L_{550}. The model assumes $\Delta E_M = \Delta E_{M_1} = \Delta E_{M_2}$ (see text). ΔE_M and ΔE_O represent the molar internal energy changes of M and O with respect to the ground state. The magnitude of ΔE_M and ΔE_O in the figure are arbitrary.

were assumed to be first-order reactions characterized by the rate constants k_1, k_2, and k_3. M should be considered as a generic representation of the two states, M_1 and M_2, which both absorb at 412 nm (7). The interconversion between the two species is described by the rate constants k_f and k_r. The parameter α evaluates the equilibrium between M_1 and M_2 ($M_2 = \alpha M$; $M_1 = [1 - \alpha]M$; $\alpha = k_f/k_r + k_f$). M_1 goes back straight to BR_{570}, whereas M_2 decays via O_{660}. The lower part of Fig. 6 shows the energetic scheme. ΔE_M and ΔE_O represent the molar internal energy changes of M_{412} and O_{660} with respect to the bacteriorhodopsin ground state. The model assumes $\Delta E_{M_1} = \Delta E_{M_2} = \Delta E_M$.

The differential equation that describes the variation of M_{412} concentration can be written

$$\frac{dM}{dt} = \phi I - \alpha k_1 M - (1 - \alpha) k_3 M, \tag{4}$$

where ϕ is the photochemical quantum yield, and I the absorbed light intensity. The differential equation corresponding to O_{660} is given by

$$\frac{dO}{dt} = \alpha k_1 M - k_2 O. \tag{5}$$

The light source is modulated, and I is a function of the chopping angular velocity, ω. Since the lock-in is sensitive to the first harmonic of the Fourier series of the response, the general solution of M and O can be written as a sum over a sinusoidal and a cosinusoidal term. By substitution of this solution into Eqs. 4 and 5, the coefficients can be evaluated. The PA signal can be analyzed in terms of the thermodynamic parameters of the photochemical reactions. The rate of heat production (Q) is equal to the absorbed light energy flux minus the rate of energy stored in the photochemical products. The energy stored in M and O at time t is given by

$$E(t) = M(t) \cdot \Delta E_M + O(t) \cdot \Delta E_O, \tag{6}$$

where ΔE_M and ΔE_O represent the molar internal energy changes of M_{412} and O_{660} with respect to the ground state (Fig. 6), whereas $M(t)$ and $O(t)$ are the molar concentrations at time t. The heat production rate (Q) can thus be written

$$Q = Nh\nu I - \Delta E_M \frac{dM}{dt} - \Delta E_O \frac{dO}{dt}. \tag{7}$$

Since $\rho = K(\omega) \cdot Q$, it follows that $\rho/\rho_{ref} = Q/Q_{ref}$. The in-phase signal is actually the sinusoidal component of Q/Q_{ref}. Eq. 8 is obtained by substituting in Eq. 7 the dM/dt and dO/dt expressions expressed in terms of the sin and cos coefficients

$$\left(\frac{Q}{Q_{ref}}\right)_{in} = 1 - \phi \frac{\Delta E_M}{Nh\nu} + \phi \frac{\Delta E_M}{Nh\nu} \frac{[\alpha k_1 + (1 - \alpha)k_3]^2}{\omega^2 + [\alpha k_1 + (1 - \alpha)k_3]^2}$$
$$- \frac{\Delta E_O}{Nh\nu} \frac{\phi \alpha k_1 \omega^2}{\omega^2 + k_2^2} \frac{\alpha k_1 + (1 - \alpha)k_3 + k_2}{\omega^2 + [\alpha k_1 + (1 - \alpha)k_3]^2}. \tag{8}$$

This equation serves to simulate the PA frequency spectra associated with the photosystem described in Fig. 6.

Estimation of the Parameters

The simulation procedure depends on seven parameters (Eq. 8). $\phi = 0.3$ is a good estimate of the quantum yield value (21–24), and several reports have shown that ϕ is pH independent (16, 25, 26). The evaluation of α is more difficult. Sherman et al. (7) have estimated this parameter assuming that the extinction coefficients of M_{412} and O_{660} were even. Recently, the ratios between α(pH 5.1)/α(pH 7.0) and α(pH 7.0)/α(pH 8.7) were measured (8). However, up to now, no absolute value of α is available. k_2 has been evaluated as a function of pH (8), but k_1 and k_3 have not been determined in experimental conditions similar to ours. Concerning M_{412}, Sherman et al. (7) observed a single rate constant at pH 5 and 7. This would imply $k_1 = k_3$ or alternatively $k_1 \gg k_3$. At pH 9.0, they observed that the M_{412} decay is biphasic and that the rate constant ratio is equal to 2.0 (7).

Considering the unknown values that appear in Eq. 8, an hypothesis had to be made to perform the simulations: at pH 5.1, α was assumed equal to 1.0 with $k_3 \ll k_1$. Consequently α(pH 7.0) = 0.85 ($k_3 \ll k_1$) and α(pH 8.9) = 0.41 ($k_3 = 2\,k_1$) (8). In absence of precise k_1 values, the PA results were used as an approximation. The values adopted for the simulations are given in Table II.

Simulation of the Experimental Curves

Fig. 7 compares the simulated curves with the experimental points at pH's 5.1, 7.0, and 8.9. The best least-square fit was obtained at pH 8.9 since $R = 0.994$, whereas it amounts to 0.975 and 0.988, respectively, at pH's 5.1 and 7.0. Only one transition is detected in the simulated curves due to the fact that k_1 and k_2 fall in the same order of magnitude (8). The discrepancy between the simulated and the experimental data is understandable considering the model simplicity and the approximations involved in the evaluation of the parameters. Simulation of various theoretical models will be discussed elsewhere (8).

The simulation provides an estimation of the enthalpy changes associated with the intermediates M_{412} and O_{660} (Table III). In the data analysis, it is assumed that the total amount of light energy absorbed by the sample (210 kJ/E [einstein]) is actually used in the photocycle, i.e., stored by the intermediates. It can be seen that ΔE_M is not significantly influenced by pH contrary to ΔE_O that, at pH 8.9, drops at 50% of its pH 5.1 value. On the other hand, if α is assumed equal to 1 at pH 8.9, $\Delta E_O = 0.08$ and this would correspond to $|\Delta E| = 4$ kcal/mol. If k_1/k_3 is assumed equal

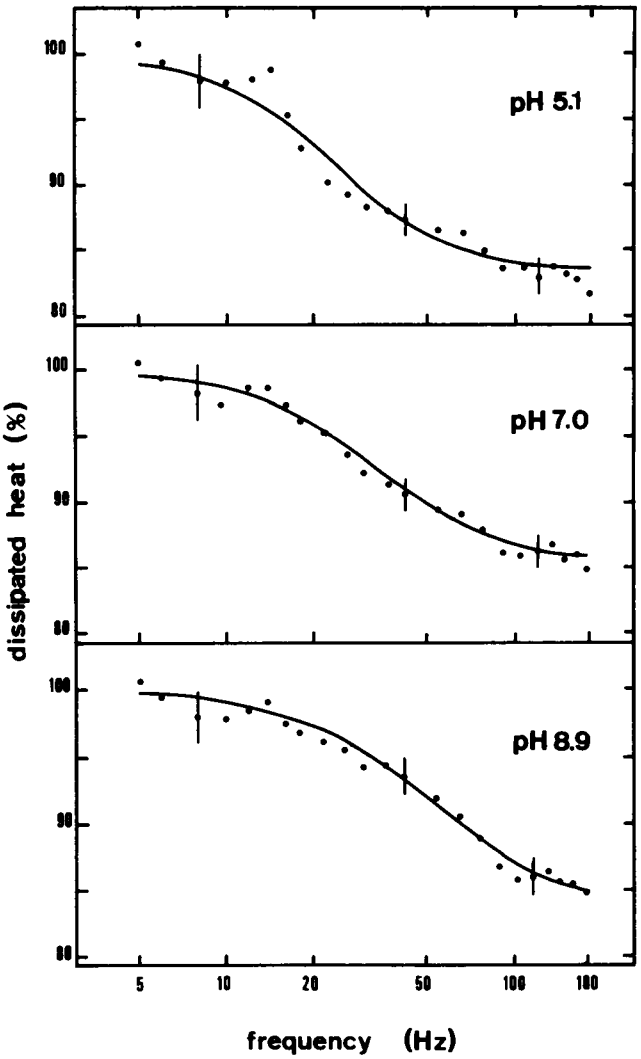

FIGURE 7 Comparison between the experimental and simulated frequency spectra of purple membrane suspensions at pH's 5.1, 7.0, and 8.9 in 66 mM buffers. The parameters values are given in Table II; pH 5.1, $R = 0.975$; pH 7.0, $R = 0.988$; pH 8.9, $R = 0.994$.

TABLE II
PARAMETER VALUES USED FOR THE SIMULATION OF THE PA FREQUENCY SPECTRA

	pH 5.1	pH 7.0	pH 8.9
ϕ	0.3	0.3	0.3
α	1	0.85	0.41
$k_1(s^{-1})$	503	506	225
$k_2(s^{-1})$	150	193	112
$k_3(s^{-1})$	0	0	450

TABLE III
COMPARISON BETWEEN THE EXPERIMENTAL AND SIMULATED VALUES OF THE MOLAR ENTHALPY CHANGES OF M_{412} AND O_{660}

		pH 5.1	pH 7.0	pH 8.9
ΔE_M	Experimental	26	22.1	23
(kcal · mol^{-1})	Simulated	26.7	24	26.5
ΔE_O	Experimental	21.1	18.1	—
(kcal · mol^{-1})	Simulated	19.6	11.8	9.3

to 2, ΔE_0 is 0.04, and this would represent an even smaller internal energy variation.

DISCUSSION

The experimental technique adopted in the present study has been outlined by Garty et al. (10). The PA frequency spectra described here are comparable with those published previously (10, 11, 19). The similarity is striking at frequencies higher than 70 Hz. By contrast, at lower frequencies, significant differences are noticeable. At low ionic strength, we observed an exothermic 21-Hz transition at the three pHs tested. An endothermic transition was detected by Garty et al. (10, 11) at pH's 7.0 and 9.9 at 30 Hz, but this transition was not reported in another paper (19). Both situations were actually observed by this group (Dr. D. Cahen, personal communication). In our study, we never detected an endothermic low frequency transition. This partial discrepancy remains unexplained. As compared with the results previously published (10, 19), our experiments were performed with a slightly higher membrane concentration (7.5×10^{-4} M against 4.8×10^{-4} M), a lower intensity of light (110 W/m^2 against 250 W/m^2). The microphone has good characteristics in the low frequency domain.

The conclusions that can be drawn from Fig. 2 concerning the photocycle kinetics overlap those deduced from Fig. 1. However, the Fig. 2 data allow the computation of the quadrature signal. To the best of our knowledge, this represents the first experimental support to the theoretical analysis carried out by Malkin and Cahen (12).

Significant errors can be introduced in the evaluation of the intermediate lifetimes from PA frequency spectra (Figs. 1, 2, 4, and 5) especially when several transitions are present at frequencies close to one another (8, 10). Nevertheless the O_{660} lifetimes deduced from the PA spectra (Table I) at pH's 5.1, 7.0, and 8.9 are in good agreement with flash photolysis results. Indeed the lifetimes were found equal to 6.7 ms at pH 5.1, 5.2 ms at pH 7.0, and 9.1 ms at pH 8.9 (8). The shortest value was observed at pH 7.0 and this is also in agreement with PA data.

The ratio of dissipated heat between the photoactive and inactive samples is proportional to $\phi \cdot \Delta E$. The plateaus that appear in the PA frequency spectra allow an estimation of the internal energy changes associated with the intermediate formation. The internal energy variations are identified with the enthalpy changes since the volume and pressure variations during the photocycle are negligible (10) and since no electric work is performed. The M_{412} plateaus and the corresponding $\phi \cdot \Delta E$ are pH independent. Since the photochemical quantum yield is constant in the 5–9 pH range (16, 26, 27), it implies that the M_{412} enthalpy is unaffected by pH (Table III).

Figs. 1 and 2 show that the O_{660} transition is very sensitive to pH. This corresponds to an effect either on the enthalpy of the reaction and/or on the amount of O_{660} formed. The pH effect on O_{660} was also observed by flash photolysis (7, 8). This justifies the branched model chosen in the present study. This model (Fig. 6) does not satisfy all criteria imposed by the spectroscopic data available (3), but it integrates the pH dependence of O_{660} and the dual pathway in the decay of M_{412} (7, 8, 20).

Table III compares the values of ΔE_M and ΔE_O obtained experimentally with those deduced from the simulation. The experimental data are expressed in kilocalories per mole assuming that each plateau corresponds to $\phi \cdot \Delta E$ (10). The pH effect concerns ΔE_O at pH 5.1, the agreement is satisfactory as expected since at this pH $\alpha = 1$. At pH 7.0, the influence of the branching is important and ΔE_O (simulated) differs markedly from ΔE_O (experimental). ΔE_O (experimental) represents a straightforward evaluation of the enthalpy variations, i.e., a value associated with an unbranched model. At pH 8.9, E_O is unmeasurable experimentally (Fig. 1), and the simulated value is significantly smaller than at pH 5.1. Note that ΔE_M and ΔE_O represent global enthalpy changes in which some endothermic contributions could be implied.

At low salt concentration, an exothermic transition is detected at 215 Hz. This represents an event occurring 0.7 ms after the onset of illumination. The 215-Hz transition represents probably a protein conformational change since no intermediate has been observed with such a lifetime. The interpretation is supported by the observation of Becher et al. (18) who have shown spectrophotometrically that a conformational change was associated with the L_{550}-M_{412} transition. At high ionic strength, the 215-Hz transition becomes endothermic. The variation suggests that the amino acid residues involved in the protein modification are accessible to the aqueous medium (18). Moreover, the conformational change occurring at 4 M NaCl, represents an increase in molecular disorder since an exothermic transition implies a positive entropy change for a spontaneous reaction.

The frequency effect is much smaller at 4 M NaCl than at low ionic strength (Fig. 4). Consequently, the positions of the plateaus are difficult to determine. However, at 4 M NaCl, O_{660} is undetected at pH 8.9, the response being constant from 5 to 40 Hz. Similar observations were performed by Garty et al. (10) at 200 mM KCl (pH 7.0). On the other hand, we have observed by flash photolysis that both the decay rate constant and the concentrations of O_{660} are reduced by high ionic strength (8). In fact, O_{660} becomes undetectable at pH 8.0 and higher in 4 M NaCl (8, 28). If the M_{412} concentration is salt independent (29), the salt effect observed on the transition represents a salt-induced decrease of the enthalpy change.

When purple membrane sheets are solubilized in detergent, the transitions are smaller than in the case of native membranes. Mantele et al. (30) have reported that the O_{660} concentration observed with monomers is accordingly smaller. The transition frequencies are not significantly different from those of Fig. 1. Flash photolysis data of Dencher and Heyn (17, 31) have shown that the M_{412}

lifetimes are similar in native and monomer bacteriorhodopsins. Our data on O_{660} lead to the same conclusion.

The values given in Table III are difficult to compare with other published data. Honig (32) and Birge (33) have estimated relative free energy changes associated with each intermediate, but nothing is known about the corresponding entropy variations. Flash calorimetry data reported by Ort and Parson (9) were obtained at 4°C and at this temperature, the concentration of O_{660} is almost unmeasurable. These authors observed an endothermic final event in the photocycle, but the intermediate identification is difficult due to the temperature of the experiments and the lack of kinetic data. Recall, however, that an endothermic transition was observed by Garty et al. (10, 11) in the low frequency region of their PA spectra. On the other hand, Cooper and Converse (34) measured the enthalpy change associated with the Meta I-Meta II conversion in bovine rhodopsin. The absolute value is similar to our data relative to the M_{412}-O_{660} transition but the Meta I-Meta II transition represents an endothermic process.

We wish to thank Professor A. Van de Vorst for his interest in this work. This work was supported by Fonds National de la Recherche Scientifique.

Received for publication 14 December 1982 and in final form 27 June 1983.

REFERENCES

1. Stoeckenius, W., R. H. Lozier, and R. A. Bogomolni. 1979. Bacteriorhodopsin and the purple membrane of Halobacteria. *Biochim. Biophys. Acta.* 505:215–278.
2. Ottolenghi, M. 1980. The photochemistry of rhodopsins. *Advan. Photochem.* 12:97–200.
3. Nagle, J. F., L. A. Parodi, and R. H. Lozier. 1982. Procedure for testing kinetic models of the photocycle of bacteriorhodopsin. *Biophys. J.* 38:161–174.
4. Lozier, R. H., R. A. Bogomolni, and W. Stoeckenius. 1975. Bacteriorhodopsin: a light-driven proton pump in *Halobacterium halobium. Biophys. J.* 15:955–962.
5. Dencher, N., and M. Wilms. 1975. Flash photometric experiments on the photochemical cycle of bacteriorhodopsin. *Biophys. Struct. Mechanism.* 1:259–271.
6. Lozier, R. H., W. Niederberger, M. Ottolenghi, G. Sivorinovsky, and W. Stoeckenius. 1978. On the photocycles of light- and dark-adapted bacteriorhodopsin. *In* Energetics and Structure of Halophilic Microorganisms. S. R. Caplan and M. Ginzburg, editors. Elsevier North-Holland, Inc., Amsterdam-New York. 123–141.
7. Sherman, W. V., R. R. Eicke, S. R. Stafford, and D. W. Wasacz. 1979. Branching in the bacteriorhodopsin photochemical cycle. *Photochem. Photobiol.* 30:727–729.
8. Renard, M., and M. Delmelle. 1983. *J. Physique.* In press.
9. Ort, D. R., and W. W. Parson. 1979. Enthalpy changes during the photochemical cycle of bacteriorhodopsin. *Biophys. J.* 25:355–364.
10. Garty, H., S. R. Caplan, and D. Cahen. 1982. Photoacoustic photocalorimetry and spectroscopy of *Halobacterium halobium* purple membranes. *Biophys. J.* 37:405–415.
11. Garty, H., D. Cahen, and S. R. Caplan. 1980. Photoacoustic calorimetry of *Halobacterium halobium* photocycle. *Biochem. Biophys. Res. Commun.* 97:200–206.
12. Malkin, S., and D. Cahen. 1979. Photoacoustic spectroscopy and radiant energy conversion: theory of the effect with spectial emphasis on photosynthesis. *Photochem. Photobiol.* 29:803–813.
13. Ducharme, D., A. Tessier, and R. M. Leblanc. 1979. Design and characteristics of a cell for photoacoustic spectroscopy of condensed matter. *Rev. Sci. Instrum.* 50:1461–1462.
14. Rosencwaig, A. 1980. Photoacoustics and photoacoustic spectroscopy. John Wiley & Sons, Inc., New York. 309.
15. Renard, M., and M. Delmelle. 1980. Quantum efficiency of light-driven proton extrusion in *Halobacterium halobium.* pH dependence. *Biophys. J.* 32:993–1006.
16. Renard, M., and M. Delmelle. 1981. The photochemical quantum yield of bacteriorhodopsin is pH independent. A photoacoustic study. *FEBS (Fed. Eur. Biochem. Soc.) Lett.* 128:245–248.
17. Dencher, N. A., and M. P. Heyn. 1978. Formation and properties of bacteriorhodopsin monomers in the non-ionic detergents octyl-β-D-glucoside and Triton X-100. *FEBS (Fed. Eur. Biochem. Soc.) Lett.* 96:322–326.
18. Becher, B., F. Tokunaga, and T. G. Ebrey. 1978. Ultraviolet and visible absorption spectra of the purple membrane protein and the photocycle intermediates. *Biochemistry.* 17:2293–2300.
19. LeGrange, J., D. Cahen, and S. R. Caplan. 1982. Photoacoustic calorimetry of purple membrane. *Biophys. J.* 37:4–6.
20. Korenstein, R., B. Hess, and D. Kuschmitz. 1978. Branching reactions in the photocycle of bacteriorhodopsin. *FEBS (Fed. Eur. Biochem. Soc.) Lett.* 93:266–270.
21. Goldschmidt, C. R., M. Ottolenghi, and R. Korenstein. 1976. On the primary quantum yields in the bacteriorhodopsin photocycle. *Biophys. J.* 16:839–843.
22. Goldschmidt, C. R., O. Kalisky, T. Rosenfeld, and M. Ottolenghi. 1977. The quantum efficiency of the bacteriorhodopsin photocycle. *Biophys. J.* 17:179–183.
23. Becher, B., and T. G. Ebrey. 1977. The quantum efficiency for the photochemical conversion of the purple membrane protein. *Biophys. J.* 17:185–191.
24. Hurley, J. B., and T. G. Ebrey. 1978. Energy transfer in the purple membrane of *Halobacterium halobrium. Biophys. J.* 22:49–66.
25. Kalisky, O., and M. Ottolenghi. 1982. Branching pathways in the photocycle of bacteriorhodopsin. *Photochem. Photobiol.* 35:109–115.
26. Rosenbach, V., R. Goldberg, C. Gilon, and M. Ottolenghi. 1982. On the role of tyrosine in the photocycle of bacteriorhodopsin. *Photochem. Photobiol.* 36:197–201.
27. Kaliski, O., and M. Ottolenghi. 1982. Branching pathways in the photocycle of bacteriorhodopsin. *Photochem. Photobiol.* 35:109–115.
28. Korenstein, R., and B. Hess. 1977. Hydratation effects on the photocycle of bacteriorhodopsin in thin layers of purple membrane. *Nature (Lond.).* 270:184–186.
29. Govindjee, R., T. G. Ebrey, and A. R. Crofts. 1980. The quantum efficiency of proton pumping by the purple membrane of *Halobacterium halobium. Biophys. J.* 30:231–242.
30. Mantele, W., F. Siebert, and W. Kreutz. 1981. Effect of Triton X-100 and of deuteration on the amplitude of the O_{640}-intermediate in the bacteriorhodopsin photocycle. *FEBS (Fed. Eur. Biochem. Soc.) Lett.* 128:249–254.
31. Dencher, N. A., and M. P. Heyn. 1979. Bacteriorhodopsin monomers pump protons. *FEBS (Fed. Eur. Biochem. Soc.) Lett.* 108:307–310.
32. Honig, B. 1978. Light energy transduction in visual pigments and bacteriorhodopsin. *Annu. Rev. Phys. Chem.* 29:31–57.
33. Birge, R. R. 1981. Photophysics of light transduction in rhodopsin and bacteriorhodopsin. *Annu. Rev. Biophys. Bioeng.* 10:315–354.
34. Cooper, A., and C. A. Converse. 1976. Energetics of primary processes in visual excitation: photocalorimetry of rhodopsin in rod outer segment membranes. *Biochemistry.* 15:2970–2978.